Fingerprint of the inverse Rashba-Edelstein effect at heavy-metal/Cu interfaces

Rui Yu,[1,*] Bingfeng Miao,[1,2,*] Qi Liu,[1] Kang He,[1] Weishan Xue,[3] Liang Sun,[1,2]
Mingzhong Wu,[4] Yizheng Wu,[2,5] Zhe Yuan,[3,†] and Haifeng Ding[1,2,‡]

[1]*National Laboratory of Solid State Microstructures and Department of Physics, Nanjing University, Nanjing, People's Republic of China*
[2]*Collaborative Innovation Center of Advanced Microstructures, Nanjing, People's Republic of China*
[3]*Center for Advanced Quantum Studies and Department of Physics, Beijing Normal University, Beijing 100875, People's Republic of China*
[4]*Department of Physics, Colorado State University, Fort Collins, Colorado 80523, USA*
[5]*Department of Physics, Fudan University, 220 Handan Road, Shanghai 200433, People's Republic of China*

(Received 10 March 2020; revised 16 September 2020; accepted 17 September 2020; published 12 October 2020)

We report the direct observation of the fingerprint of the inverse Rashba-Edelstein effect (IREE) via investigations of the spin-to-charge conversion in Ta(Pt)/Cu and Cu/Ta(Pt) as a function of the heavy-metal thickness. The converted charge voltages have opposite signs for samples with reversed stacking orders in the ultrathin regime and have the same sign at higher thickness. The effect is demonstrated with two independent experimental approaches and supported by first-principles calculations. Our observations unambiguously demonstrate the existence of the IREE at heavy-metal/Cu interfaces and provide a framework for manipulating the spin-charge conversion via interface engineering.

DOI: 10.1103/PhysRevB.102.144415

Spintronics has relied on exchange interactions between conduction electrons and localized spins in magnetic materials to create spin-polarized currents, or to manipulate the magnetization via the spin-transfer torque [1–3]. Subsequently, interest has centered on the generation and manipulation of pure spin current, which is not accompanied by a net charge current and corresponding stray field. The generation and detection of the pure spin current generally occur in materials with spin-orbit coupling (SOC), both in the bulk and at the surface/interface. In the bulk, the effect is referred to as the spin Hall effect (SHE) and its reciprocal the inverse spin Hall effect (ISHE), depending on whether it converts charge current $\vec{J}_C$ to spin current $\vec{J}_S$ or vice versa [4,5]. At the surface/interface, the Rashba-Edelstein effect (REE) or the inverse Rashba-Edelstein effect (IREE) [6–8] has similar functionality. While the SHE/ISHE has been extensively discussed among different materials, the REE/IREE has only recently been reported and remains hotly debated.

REE was previously invoked to explain the sign change of the spin-orbit torque effective fields in Ta/CoFeB/MgO with ultrathin Ta thickness [9]. However, the transport behavior of metallic ferromagnet is nontrivial. Other possible contributions such as anomalous Hall torque [10], planar Hall torque [11], spin-swapping torque [12], and magnetization-independent SHE torque [13] need to be carefully excluded. The first experimental report of the IREE at metallic interface was conducted by Rojas Sánchez *et al.*, where the spin-to-charge conversion in pure Bi, pure Ag, and Bi/Ag bilayer were compared utilizing the spin-pumping technique [14]. The authors found a surprisingly large enhancement of the converted charge current in Bi/Ag bilayer as compared to Bi or Ag single layer and attributed it to the IREE at the Bi/Ag interface. Their report stimulated several investigations on interfaces between metals [15–19]. Interestingly, using the spin Seebeck effect (SSE), another commonly used spin-injection technique, Yue *et al.*, however, observed a negligibly small IREE at the Bi/Ag interface [20], in sharp contrast to previous findings. It was also pointed out that the spurious effects in metallic ferromagnet and multiple carriers of Bi thin film may complicate the analysis [21,22]. Beside metallic interfaces, the IREE has also been reported in two-dimensional (2D) electron gases formed at the $SrTiO_3/LaAlO_3$ interface but the intrinsic mechanism also remains in debate [23–25]. In short, though there are interesting indirect findings attributed to the IREE, the effect is still under intense debate, especially in metallic systems, and requires direct experimental evidence.

The REE/IREE originates from the SOC at interfaces with broken inversion symmetry, namely the Rashba-type SOC [26–28]. The Hamiltonian of the Rashba-type SOC can be described as $H_R = \alpha_R(\vec{k} \times \vec{\sigma}) \cdot \vec{z}$, where α_R is the Rashba coefficient, $\vec{k}$ is the electron momentum, $\vec{\sigma}$ are the Pauli matrices, and $\vec{z}$ is the direction vector perpendicular to the interface [29,30]. In this scenario, it induces a shift of the parabolic dispersion in k space, resulting in two Fermi contours with opposite spin-momentum locking textures [Fig. 1(a)]. From the Hamiltonian, one can readily find that the spin orientations of the two Fermi contours are reversed if the stacking order reverses [Fig. 1(b)]. When a spin current with spin polarization σ_y is injected, it causes an accumulation of spin-up ($\sigma_y > 0$) electrons and a depletion of spin-down ($\sigma_y < 0$) electrons. This process shifts the two inequivalent Fermi contours, generating a transverse charge current along the x direction, hence the IREE [Fig. 1(c)]. The IREE converts a three-dimensional (3D) spin current into a 2D charge current with an efficiency

*These authors contributed equally to this work.
†zyuan@bnu.edu.cn
‡hfding@nju.edu.cn

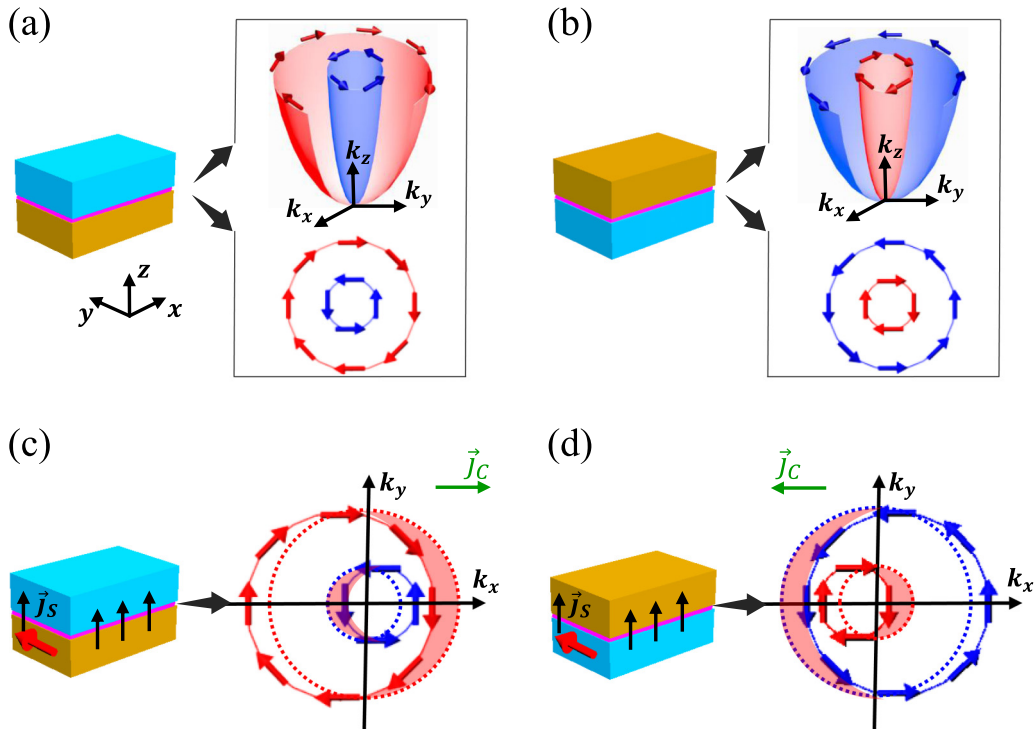

FIG. 1. (a) Schematic of the Rashba splitting and its corresponding Fermi contours with helical spin configurations of opposite helicity. (b) The Rashba splitting and spin helicity change signs when the stacking order is reversed. (c) Injection of spin current with spin polarization along y shifts the two inequivalent Fermi contours generating a transverse charge current along the x direction. (d) The generated charge current changes sign when the stacking order is reversed. Green arrows in (c) and (d) denote the directions of the generated charge currents through IREE.

denoted by $\lambda_{\mathrm{IREE}} = \frac{J_c}{J_s}$, which has the unit of length [14]. Due to the inversion symmetry-breaking nature of the Rashba Hamiltonian, the generated charge current will reverse its direction when the stacking order is reversed [Fig. 1(d)]. This feature is regarded as the fingerprint of the IREE. Previous attempts also tried to show IREE with this fingerprint but they either found the same sign, or the opposite sign only in the thick regime, in contrast to the interfacial nature of the IREE [19,31].

In this work, we report the direct observation of the fingerprint of the IREE at heavy-metal (Ta and Pt)/Cu interfaces. We prepare two series of samples with reversed stacking orders, Ta(Pt)/Cu and Cu/Ta(Pt) with different Ta(Pt) thicknesses. The charge current converted from pure spin current, injected using both spin pumping and SSE technique, shows opposite sign for samples with reversed stacking orders in the ultrathin region. The observed interfacial characteristics and sign change with reversed stacking order directly reflect the distinct nature of the IREE. The effect is further supported by control experiments and first-principles calculations. Our observations unambiguously demonstrate the existence of the IREE at Ta(Pt)/Cu interfaces, and provide a framework for manipulating the spin-charge conversion via interface engineering.

We use 30-nm-thick high-quality yttrium iron garnet (YIG) films as the spin-current injectors. Two heavy metals, Ta and Pt, are chosen as they have strong SOC but opposite signs of the spin Hall angle θ_{SH} [32]. For the sample growth and characterization details, please refer to Supplemental Material, Note 1 [33]. Figure 2(a) presents the schematic of the experiment setup for the spin-pumping measurements. The samples are placed, with the gadolinium gallium garnet substrate facing up, onto a coplanar waveguide. Under microwave excitation, the magnetization of the YIG film precesses and pumps a pure spin current into the nonmagnetic layers which is subsequently converted into a charge current via the ISHE and/or the IREE. Figure 2(b) presents typical curves of the detected dc voltage V_{sp} for YIG/Pt(5) (red) (the number in parentheses is the layer thickness in nm and hereafter) and YIG/Ta(5) (blue), where the magnetic field sweeps along the $+y$ direction. In this configuration, spin rectification is minimized [34,35] as confirmed in Supplemental Material, Note 2 [33]. As shown in Fig. 2(b), the signals detected at their resonance fields for YIG/Pt and YIG/Ta exhibit positive and negative values, consistent with their signs of θ_{SH} [32,36]. Thus, a benchmark is established to probe the sign of spin-to-charge conversion.

We then investigate the samples with opposite stacking orders, Cu/Ta(Pt) and Ta(Pt)/Cu. We fix the thickness of the Cu layer to 6 nm and perform the study as a function of the heavy-metal thickness. Figures 2(c) and 2(d) present the spin-pumping curves for YIG/Cu(6)/Ta(0.6) and YIG/Ta(0.6)/Cu(6). V_{sp} shows a positive sign for YIG/Cu(6)/Ta(0.6) but a negative sign for YIG/Ta(0.6)/Cu(6). Thus, the spin-to-charge conversion shows the fingerprint of the IREE, i.e., opposite sign for samples with reversed stack-

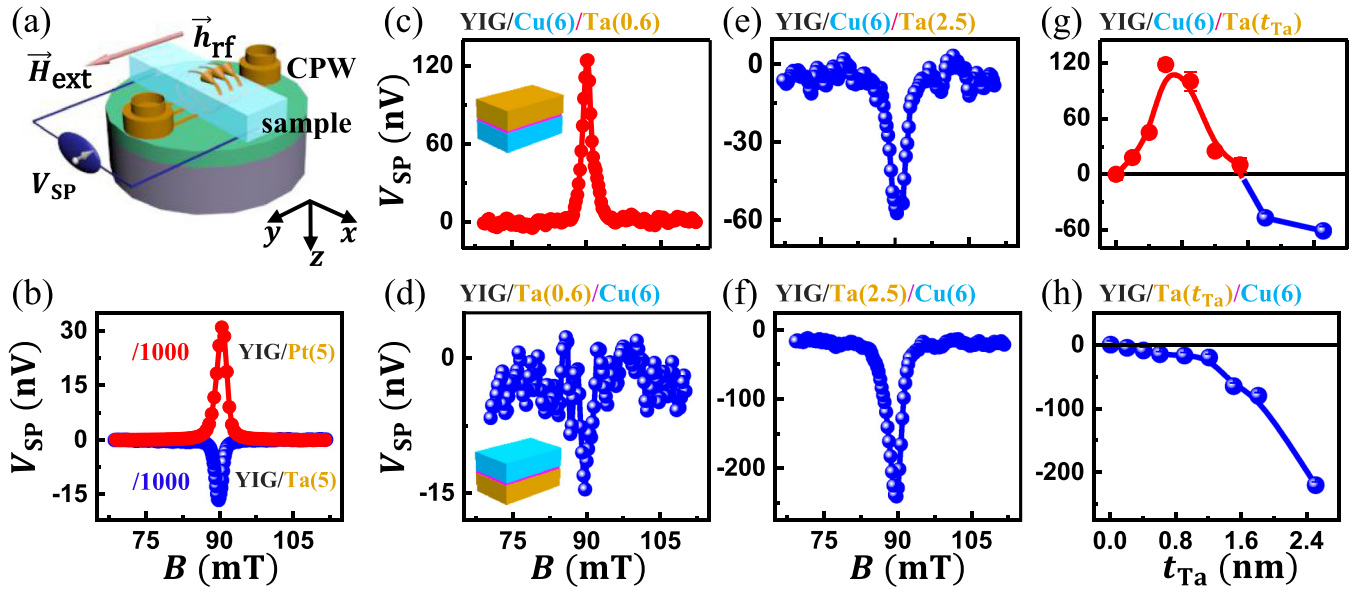

FIG. 2. (a) Schematic of the experimental setup for spin pumping. (b) Field-dependent spin-pumping voltage curves for two representative samples with opposite spin Hall angles, YIG/Pt(5) (red curve) and YIG/Ta(5) (blue curve) excited by 6-GHz microwave. The dc magnetic field is along $+y$ direction. Here, "/1000" means the signal has been divided by 1000. (c)–(f) Spin-pumping voltage curves for YIG/Cu(6)/Ta(0.6), YIG/Ta(0.6)/Cu(6), YIG/Cu(6)/Ta(2.5), YIG/Ta(2.5)/Cu(6), respectively. Ta thickness-dependent spin-pumping voltages at the resonant field for opposite stacking orders: (g) YIG/Cu(6)/Ta(t_{Ta}) and (h) YIG/Ta(t_{Ta})/Cu(6), respectively.

ing orders at ultrathin regime. With an increase of t_{Ta}, both YIG/Cu(6)/Ta(2.5) and YIG/Ta(2.5)/Cu(6) exhibit negative V_{sp} [Figs. 2(e) and 2(f)], the same sign as that of YIG/Ta(5). Note the smaller value obtained for the samples with the Cu layer is due to the shunting effect as confirmed by control experiment (Supplemental Material, Note 3 [33]).

Figures 2(g) and 2(h) summarize the t_{Ta}-dependent spin-pumping voltage for samples with reversed stacking orders (the t_{Ta}-dependent current is also provided in Supplemental Material, Note 4 [33], which exhibit essentially the same feature as the voltage data as the resistance is dominant by the Cu layer). V_{sp} has an opposite sign for all samples when $t_{Ta} <$ 1.5 nm, indicating that it is a general feature of the samples. This matches the fingerprint of the IREE as discussed above. At higher thicknesses, V_{sp} shows the same negative sign as that of the bulk ISHE of Ta. The thickness-dependent sign change of V_{sp} for Cu(6)/Ta(t_{Ta}) can be understood as the competition of the interfacial IREE and the bulk ISHE. When $t_{Ta} <$ 1.5 nm, the IREE at the Cu/Ta interface is dominant, thus V_{sp} of Cu(6)/Ta(t_{Ta}) is positive [red dots in Fig. 2(g)]. When $t_{Ta} >$ 1.5 nm, the bulk ISHE is dominant, thus V_{sp} changes its sign to negative [blue dots in Fig. 2(g)]. The initial increase of V_{sp} of Cu(6)/Ta(t_{Ta}) up to $t_{Ta} = 0.6$ nm can be explained by the gradual establishment of the Cu-Ta interface. As for Ta(t_{Ta})/Cu(6), since both the IREE of the Ta/Cu interface and the ISHE of the Ta have the same sign (negative), we only observe negative values of V_{sp} [Fig. 2(h)]. Our control experiments for YIG/Ta exclude that the sign reversal is caused by the Ta/air interface, demonstrating that the effect is indeed due to the Cu/Ta interface (Supplemental Material, Note 5 [33]).

To confirm our findings, which should be independent of the experimental technique, we also perform the spin-to-charge measurements of the same samples using the SSE [37]. Figure 3(a) presents the schematic for the SSE measurements. The samples are placed in between a heater and thermal bath, where a perpendicular temperature gradient is established. The SSE in YIG drives a spin current that flows along the z direction and enters the nonmagnetic layers, which can be detected as a voltage V_{SSE}. Figure 3(b) presents typical curves of the detected V_{SSE} for YIG/Pt(5) (red) and YIG/Ta(5) (blue). Pt (Ta) exhibits a positive (negative) V_{SSE} for positive magnetic field, and the sign of V_{SSE} changes when the field direction is reversed. Both V_{sp} and V_{SSE} are consistent in reflecting the sign of θ_{SH} for the heavy metals.

After establishing this benchmark, we performed the SSE measurements for samples with reversed stack orders and different t_{Ta} (Supplemental Material, Note 6 [33]). Similar to the spin-pumping experiments, the value of V_{SSE} of the YIG/Cu(6)/Ta(t_{Ta}) sample first increases with t_{Ta}, reaches a peak value at ~0.6 nm, and then gradually decreases and changes sign to negative at ~1.5 nm [Fig. 3(c)]. V_{SSE} is always negative in YIG/Ta(t_{Ta})/Cu(6) in the investigated thickness range [Fig. 3(d)]. The SSE measurements reproduce all features observed in the spin-pumping measurements. Thus, the fingerprint of the IREE, opposite signs for interfaces with reversed stacking orders in the ultrathin regime, is observed via both techniques for the Cu-Ta interface.

We also performed a control experiment with a designed Cu/Ta/Cu trilayer system. As discussed above, YIG/Cu(6)/Ta(0.9) possesses a positive spin-pumping voltage due to the dominant positive interfacial IREE contribution [Fig. 3(e)]. Adding another Cu layer on top of the Ta will introduce an additional Ta/Cu interface. If this interface has the negative λ_{IREE} (opposite to Cu/Ta interface), it will weaken the total IREE contribution, and the sign of the measured signal may change to negative as the bulk ISHE dominates. Indeed, V_{sp} of YIG/Cu(6)/Ta(0.9)/Cu(6) changes sign to neg-

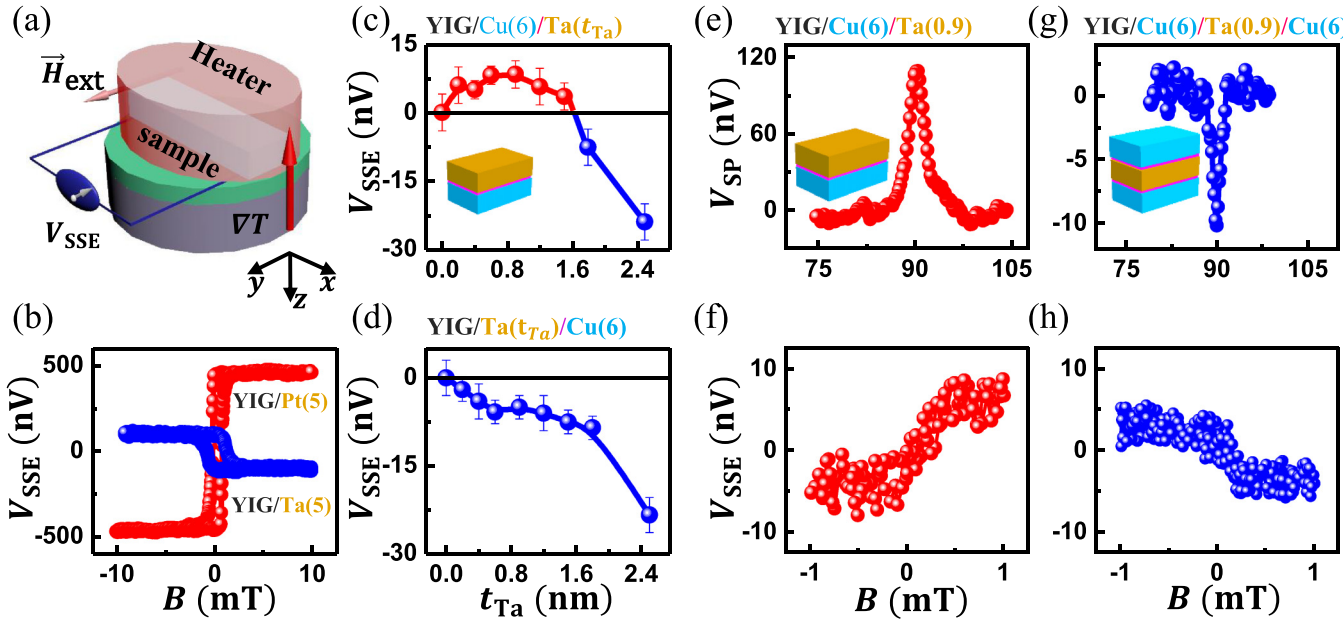

FIG. 3. (a) Schematic of the experimental setup for SSE. (b) Field-dependent SSE curves for YIG/Pt(5) (red curve) and YIG/Ta(5) (blue curve). Ta thickness-dependent SSE amplitude for opposite stacking orders: (c) YIG/Cu(6)/Ta(t_{Ta}) and (d) YIG/Ta(t_{Ta})/Cu(6), respectively. (e), (f) Spin pumping and SSE curves for YIG/Cu(6)/Ta(0.9), respectively. (g), (h) Spin pumping and SSE curves for YIG/Cu(6)/Ta(0.9)/Cu(6), respectively.

ative [Fig. 3(g)]. Thermal measurements exhibit the same behavior, as shown in Figs. 3(f) and 3(h). The spin-to-charge conversion in Cu/Ta/Cu trilayer changes its sign at thinner Ta thickness (∼0.6 nm) as compared to the Cu/Ta bilayer system (∼1.5 nm) due to the added Ta/Cu interface. This further confirms that the Cu/Ta and Ta/Cu interfaces have the opposite sign in spin-charge conversion, consistent with the IREE fingerprint.

In addition to Ta, Pt is also a heavy metal with strong SOC, albeit with a positive value of the θ_{SH} [32], and has been widely studied in the detection of spin currents and in magnetization switching with spin-orbit torque [38–42]. We thus performed similar measurements on the Cu/Pt system. The spin-to-charge conversion in YIG/Cu(6)/Pt(t_{Pt}) shows a negative sign when $t_{Pt} < 0.4$ nm and changes to positive sign with further increase of t_{Pt}. In YIG/Pt(t_{Pt})/Cu(6), it is always positive in the whole thickness range that we investigated (Supplemental Material, Note 7 [33]). These findings reveal an IREE also exists in the Pt-Cu interface. We note that Cu has been widely used as an inserted layer in spin-transport studies [42–46]. In these references, the Pt films used are however too thick to observe the sign change. In addition, the influence of composition in CuTa(Pt) alloys on the sign of spin Hall angle can be ruled out (Supplemental Material, Note 8 [33]).

As discussed above, the spin-charge conversion changes sign at ∼1.5 nm for YIG/Cu/Ta. We defined the critical thickness as t_c. where the ISHE and IREE canceled each other. We can use it to make a rough estimation with a simplified model, $\lambda_{IREE} = 1/2\theta_{SH}t_c$ [14]. The characterization of θ_{SH} of normal metals is very important, albeit still highly debated. Choosing $\theta_{SH} = -0.0062$ for Ta [36], we obtain $\lambda_{IREE} = 0.005$ nm for Cu/Ta interfaces. It is important to point out that the esitimated λ_{IREE} is propotional with spin Hall angle θ_{SH}. If one chooses $\theta_{SH}(\mathrm{Ta}) = -0.15$ [47], $\lambda_{IREE}(\mathrm{Cu/Ta}) = 0.12$ nm. Note that this rough estimate ignores the effect of the interface spin loss.

To include the spin loss at the interface between Cu and Ta and bulk contribution from ISHE, we follow the model proposed by Chen and Zhang [48,49], where the effective spin-mixing conductance is

$$g_{\mathrm{eff}}^{\uparrow\downarrow} = G^{\uparrow\downarrow}[1-(1-\delta)^2\varepsilon]. \quad (1)$$

δ represents the spin-memory loss factor, $\varepsilon = \frac{G^{\uparrow\downarrow}}{G^{\uparrow\downarrow}+(2/3)k_F^2(\lambda_{mf}/\lambda_{sd})\tanh(t_N/\lambda_{sd})}$ characterizes the spin backflow, and k_F is the Fermi vector of the Ta layer. The spin current transmitted into Ta is $G^{\uparrow\downarrow}(1-\varepsilon)(1-\delta)$, which converts into charge current via ISHE; and the spin current absorbed by the interface is $G^{\uparrow\downarrow}(1+\varepsilon-\varepsilon\delta)\delta$, which converts into charge current via IREE. Then, the normalized spin-pumping voltage can be written as

$$\frac{V_{SP}}{\alpha\beta ewfR} = \lambda_{IREE}G^{\uparrow\downarrow}(1+\varepsilon-\varepsilon\delta)\delta + G^{\uparrow\downarrow}(1-\varepsilon)(1-\delta)\theta_{SH}\lambda_{sd}\tanh\left(\frac{t_N}{2\lambda_{sd}}\right), \quad (2)$$

where α, β is the in-plane and out-of-plane precessing angle of YIG, respectively, w is the width of the sample, f is the microwave frequency, R is the resistance of the sample, and t_N is the thickness of Ta.

Experimentally, the effective spin-mixing conductance can be obtained with $g_{\mathrm{eff}}^{\uparrow\downarrow} = (4\pi M_S t_F/g\mu_B)(\alpha_{F/N}-\alpha_F)$, where $4\pi M_S$ is the saturation magnetization, t_F is the thickness of the ferromagnetic layer, g is the Landé factor, μ_B is the Bohr magnetron, and $\alpha_{F/N}$ and α_F represent the damping constant for the YIG/Cu/Ta and YIG, respectively. Saturation magnetization can be obtained from the resonance field H_R-dependent

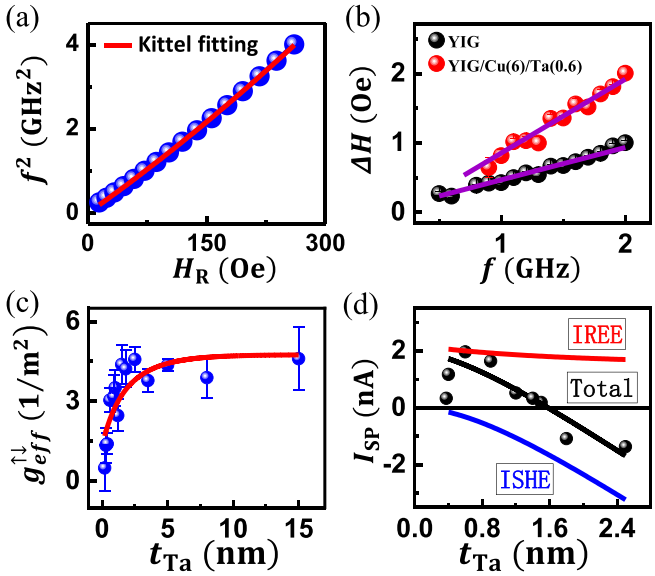

FIG. 4. (a) The square of the frequency vs ferromagnetic resonance field for YIG. The red line is the fit using the Kittel equation. (b) The half linewidth vs frequency for YIG (black) and YIG/Cu(6)/Ta(0.6) (red), respectively. The lines are linear fittings. (c) Thickness-dependent effective spin-mixing conductance for YIG(30)/Cu(6)/Ta(t_{Ta}). The blue symbols are the experimental data and the red lines are the fittings. (d) Comparison of the contributions from IREE and ISHE for YIG/Cu(6)/Ta(t_{Ta}). The symbols are the experimental data and the lines are the fittings.

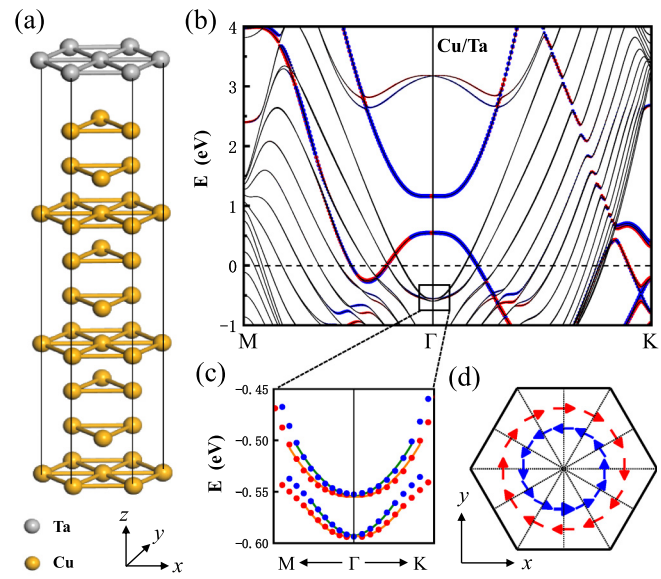

FIG. 5. (a) Schematic illustration of the bilayer geometry in the calculation. (b) Calculated energy bands near the Fermi energy of Cu/Ta with one atomic layer of Ta on top of Cu. The size of the symbols represents the contribution of the interfacial Cu and Ta layers. The red and blue symbols denote the spin-splitting states whose in-plane spin components have a clockwise and counterclockwise circulation, respectively. The thick orange and green lines are the fittings using the analytical Rashba model. (c) Magnified plot for the Rashba bands yielding $\alpha_R = 0.09$ eV Å (upper) and $\alpha_R = 0.13$ eV Å (lower). (d) The distribution of projected in-plane spin components for the Rashba splitting states shown in (c).

microwave frequency f [Fig. 4(a)]. Fitting the Kittel equation $f^2 = (\gamma/2\pi)^2(H_R)(H_R + 4\pi M_S)$ yields $4\pi M_S = 1689G$. The damping constants are obtained from the slope of the ferromagnetic resonance half-linewidth ΔH as a function of f, $\Delta H = \Delta H_0 + \alpha f \frac{2\pi}{\gamma}$ [Fig. 4(b)], where $\frac{\gamma}{2\pi} \approx 2.8$ GHz/kOe is the gyromagnetic ratio. We obtain the damping constants for YIG, YIG/Cu(6)/Ta(0.6) as $\alpha_{YIG} = (1.3 \pm 0.1) \times 10^{-3}$, and $\alpha_{YIG/Cu/Ta} = (2.6 \pm 0.1) \times 10^{-3}$, respectively. Therefore, $g^{\uparrow\downarrow}_{\text{eff}}$ for YIG/Cu(6)/Ta(0.6) can be calculated as $(3.4 \pm 0.5) \times 10^{18}$m^{-2}. The values is comparable with those reported in the literature [40]. Fitting the Ta thickness-dependent effective spin-mixing conductance experimental data [Fig. 4(c)], we obtain $G^{\uparrow\downarrow} = (6.4 \pm 0.9) \times 10^{18}$ m^{-2} and the spin-loss factor $\delta = 0.11 \pm 0.04$. In the calculation, we chose $k_F = 5.3$ nm [50], $\lambda_{mf} = 3.7$ nm, and $\lambda_{sd} = 5.1$ nm [36].

At the critical thickness t_c, the ISHE and IREE cancel. Equation (2) can be rewritten as

$$\lambda_{\text{IREE}}(1+\varepsilon-\varepsilon\delta)\delta + (1-\varepsilon)(1-\delta)\theta_{\text{SH}}\lambda_{sd}\tanh\left(\frac{t_c}{2\lambda_{sd}}\right) = 0 \tag{3}$$

By taking the fitting results shown above, and $\theta_{\text{SH}} = -0.006$ reported in the reference [36], we can obtain the Rashba length for the Cu/Ta interface as $\lambda_{\text{IREE}}(\text{Cu/Ta}) = (0.0090 \pm 0.0013)$ nm. Again, if larger value of θ_{SH} of Ta is chosen, we can obtain $\lambda_{\text{IREE}}(\text{Cu/Ta}) = (0.22 \pm 0.03)$ nm. With the above fitting parameters, we can separate the interface IREE and bulk ISHE contributions with Eq. (2), as presented in Fig. 4(d). For YIG/Cu(6)/Ta(t_{Ta}), the IREE is positive and the ISHE is negative. We do the same procedure for Cu/Pt interface (Supplemental Material, Note 9 [33]).

To gain a microscopic understanding of the experimental observation, we calculate the electronic structure of Cu/Ta and Cu/Pt interfaces via density-functional theory. We first construct a thin film consisting of 13 atomic layers of fcc Cu oriented along (111), on top of which another one to three atomic layers of Ta (Pt) are added [Fig. 5(a)]. The in-plane lattice constant of the Ta (Pt) layers is kept the same as that of the fcc Cu. Perpendicular to the interface, the distance between neighboring atomic layers in Ta (Pt) is chosen to keep the atomic volume conserved, as in corresponding equilibrium bulk structures. The electronic structure is self-consistently calculated using a plane-wave basis in combination with the projector-augmented wave method. A $20\times20\,k$-mesh is employed to sample the 2D Brillouin zone. SOC is included in the calculation. Figure 5(b) presents the calculated band structure of Cu/Ta interface with one Ta layer, where the symbol size represents the contribution of the interfacial Cu and Ta layers. These states localized at the interface usually have spin-dependent splitting owing to the enhanced SOC. The states are marked by red or blue symbols if they have clockwise or counterclockwise-oriented spin polarization in the $x-y$ plane, respectively, and the projected spin components are explicitly plotted in Fig. 5(d). The Rashba-like energy splitting appears near the Fermi energy yielding the coefficient $\alpha_R = 0.09 \sim 0.13$ eV Å, and with more Ta layers on top of Cu leads to $\alpha_R = 0.09 \sim 0.14$ eV Å.

Now we consider a spin current moving from Cu to Ta with its polarization along y. It results in an overall spin accumulation at k_x in the Brillouin zone and hence a particle current along x. Because of the negative spin Hall angle in bulk Ta, a spin current with its polarization along y moving towards the z direction leads to a particle current along $-x$. Therefore, considering the spin current injected through YIG/Cu/Ta, the measured voltages due to the IREE and ISHE are expected to be opposite, in agreement with the experimental observations. We also repeat the same calculation for the Cu/Pt interface (Supplemental Material, Note 10 [33]). Consistent with the experiments reported herein, the Rashba splitting between Cu/Pt and Cu/Ta interfaces is opposite. The calculated Rashba coefficient is $\alpha_R = -(0.25 \sim 0.42)\,\text{eV Å}$ for $1 \sim 3$ atomic layers of Pt on Cu. They are reasonably consistent with the values estimated experimentally (Supplemental Material, Note 11 [33]).

In summary, utilizing the spin-pumping and spin Seebeck effect measurements, we investigated the spin-to-charge conversion at heavy-metal (Ta and Pt)/Cu interfaces for samples with reversed stacking orders. When the thickness of heavy metal is ultrathin, we observe opposite signs in spin-to-charge conversion for samples with reversed stacking orders, which serves as the fingerprint of the IREE. We show that the sign and amplitude of the spin-to-charge conversion can be manipulated by reversing the stacking order, changing the thickness of heavy metals, or adding a capping layer. Our observations unambiguously demonstrate the existence of the IREE at heavy-metal/Cu interfaces and provide a framework for modification of the spin-charge conversion via interface engineering.

ACKNOWLEDGMENTS

This work was supported by the National Key R&D Program of China (Grants No. 2017YFA0303202 and No. 2018YFA0306004), the National Natural Science Foundation of China (Grants No. 11974165, No. 51971110, No. 11734006, No. 11727808, and No. 61774018), and the Natural Science Foundation of Jiangsu Province (Grant No. BK20190057). Work at CSU was supported by the U.S. National Science Foundation under Grants No. EFMA-1641989 and No. ECCS-1915849.

[1] S. A. Wolf, D. D. Awschalom, R. A. Buhrman, J. M. Daughton, S. von Molnár, M. L. Roukes, A. Y. Chtchelkanova, and D. M. Treger, Science **294**, 1488 (2001).
[2] D. C. Ralph and M. D. Stiles, J. Magn. Magn. Mater. **320**, 1190 (2008).
[3] S. Mangin, D. Ravelosona, J. A. Katine, M. J. Carey, B. D. Terris, and E. E. Fullerton, Nat. Mater. **5**, 210 (2006).
[4] J. Sinova, S. O. Valenzuela, J. Wunderlich, C. H. Back, and T. Jungwirth, Rev. Mod. Phys. **87**, 1213 (2015).
[5] A. Manchon, J. Železný, I. M. Miron, T. Jungwirth, J. Sinova, A. Thiaville, K. Garello, and P. Gambardella, Rev. Mod. Phys. **91**, 035004 (2019).
[6] V. M. Edelstein, Solid State Commun. **73**, 233 (1990).
[7] D. C. Vaz, A. Barthélémy, and M. Bibes, Jpn. J. Appl. Phys. **57**, 0902A4 (2018).
[8] G. Bihlmayer, O. Rader, and R. Winkler, New J. Phys. **17**, 050202 (2015).
[9] J. Kim, J. Sinha, M. Hayashi, M. Yamanouchi, S. Fukami, T. Suzuki, S. Mitani, and H. Ohno, Nat. Mater. **12**, 240 (2013).
[10] S. Iihama, T. Taniguchi, K. Yakushiji, A. Fukushima, Y. Shiota, S. Tsunegi, R. Hiramatsu, S. Yuasa, Y. Suzuki, and H. Kubota, Nat. Electron. **1**, 120 (2018).
[11] C. Safranski, E. A. Montoya, and I. N. Krivorotov, Nat. Nanotechnol. **14**, 27 (2019).
[12] C. O. Pauyac, M. Chshiev, A. Manchon, and S. A. Nikolaev, Phys. Rev. Lett. **120**, 176802 (2018).
[13] W. L. Yang, J. W. Wei, C. H. Wan, Y. W. Xing, Z. R. Yan, X. Wang, C. Fang, C. Y. Guo, G. Q. Yu, and X. F. Han, Phys. Rev. B **101**, 064412 (2020).
[14] J. C. R. Sánchez, L. Vila, G. Desfonds, S. Gambarelli, J. P. Attané, J. M. De Teresa, C. Magén, and A. Fert, Nat. Commun. **4**, 2944 (2013).
[15] M. B. Jungfleisch, Q. Zhang, W. Zhang, J. E. Pearson, R. D. Schaller, H. Wen, and A. Hoffmann, Phys. Rev. Lett. **120**, 207207 (2018).
[16] S. Sangiao, J. M. De Teresa, L. Morellon, I. Lucas, M. C. Martínez-Velarte, and M. Viret, Appl. Phys. Lett. **106**, 172403 (2015).
[17] A. Nomura, T. Tashiro, H. Nakayama, and K. Ando, Appl. Phys. Lett. **106**, 212403 (2015).
[18] W. Zhang, M. B. Jungfleisch, W. Jiang, J. E. Pearson, and A. Hoffmann, J. Appl. Phys. **117**, 17C727 (2015).
[19] C. Zhou, Y. P. Liu, Z. Wang, S. J. Ma, M. W. Jia, R. Q. Wu, L. Zhou, W. Zhang, M. K. Liu, Y. Z. Wu, and J. Qi, Phys. Rev. Lett. **121**, 086801 (2018).
[20] D. Yue, W. W. Lin, J. J. Li, X. F. Jin, and C. L. Chien, Phys. Rev. Lett. **121**, 037201 (2018).
[21] Y. Ando and M. Shiraishi, J. Phys. Soc. Jpn. **86**, 011001 (2017).
[22] M. Matsushima, S. Miwa, S. Sakamoto, T. Shinjo, R. Ohshima, Y. Ando, Y. Fuseya, and M. Shiraishi, Appl. Phys. Lett. **117**, 042407 (2020).
[23] E. Lesne, Y. Fu, S. Oyarzun, J. C. Rojas-Sánchez, D. C. Vaz, H. Naganuma, G. Sicoli, J. P. Attané, M. Jamet, E. Jacquet, J. M. George, A. Barthélémy, H. Jaffrès, A. Fert, M. Bibes, and L. Vila, Nat. Mater. **15**, 1261 (2016).
[24] Q. Song, H. Zhang, T. Su, W. Yuan, Y. Chen, W. Xing, J. Shi, J. Sun, and W. Han, Sci. Adv. **3**, e1602312 (2017).
[25] S. Ohya, D. Araki, L. D. Anh, S. Kaneta, M. Seki, H. Tabata, and M. Tanaka, Phys. Rev. Research **2**, 012014(R) (2020).
[26] Y. A. Bychkov and E. I. Rashba, JETP Lett. **39**, 78 (1984).
[27] I. M. Miron, G. Gaudin, S. Auffret, B. Rodmacq, A. Schuhl, S. Pizzini, J. Vogel, and P. Gambardella, Nat. Mater. **9**, 230 (2010).
[28] I. M. Miron, T. Moore, H. Szambolics, L. D. Buda-Prejbeanu, S. Auffret, B. Rodmacq, S. Pizzini, J. Vogel, M. Bonfim, A. Schuhl, and G. Gaudin, Nat. Mater. **10**, 419 (2011).
[29] A. Soumyanarayanan, N. Reyren, A. Fert, and C. Panagopoulos, Nature (London) **539**, 509 (2016).
[30] W. Han, Y. Otani, and S. Maekawa, npj Quantum Mater. **3**, 27 (2018).

[31] M. Matsushima, Y. Ando, S. Dushenko, R. Ohshima, R. Kumamoto, T. Shinjo, and M. Shiraishi, Appl. Phys. Lett. **110**, 072404 (2017).

[32] T. Tanaka, H. Kontani, M. Naito, T. Naito, D. S. Hirashima, K. Yamada, and J. Inoue, Phys. Rev. B **77**, 165117 (2008).

[33] See Supplemental Material at http://link.aps.org/supplemental/10.1103/PhysRevB.102.144415 for extended data of sample preparation and structure characterization, spin-charge conversion of Cu/Pt interface, estimation of the Rashba coefficient, calculation of the electronic structure of Cu/Pt interface, and other controlled experiments, which includes Refs. [14,36,43,48,49,51–69].

[34] L. H. Bai, Z. Feng, P. Hyde, H. F. Ding, and C. M. Hu, Appl. Phys. Lett. **102**, 242402 (2013).

[35] Y. S. Gui, L. H. Bai, and C. M. Hu, Sci. China Phys. Mech. **56**, 124 (2013).

[36] R. Yu, B. F. Miao, L. Sun, Q. Liu, J. Du, P. Omelchenko, B. Heinrich, M. Z. Wu, and H. F. Ding, Phys. Rev. Mater. **2**, 074406 (2018).

[37] K. Uchida, S. Takahashi, K. Harii, J. Ieda, W. Koshibae, K. Ando, S. Maekawa, and E. Saitoh, Nature (London) **455**, 778 (2008).

[38] I. M. Miron, K. Garello, G. Gaudin, P.-J. Zermatten, M. V. Costache, S. Auffret, S. Bandiera, B. Rodmacq, A. Schuhl, and P. Gambardella, Nature (London) **476**, 189 (2011).

[39] S. Y. Huang, X. Fan, D. Qu, Y. P. Chen, W. G. Wang, J. Wu, T. Y. Chen, J. Q. Xiao, and C. L. Chien, Phys. Rev. Lett. **109**, 107204 (2012).

[40] H. L. Wang, C. H. Du, Y. Pu, R. Adur, P. C. Hammel, and F. Y. Yang, Phys. Rev. Lett. **112**, 197201 (2014).

[41] L. Q. Liu, T. Moriyama, D. C. Ralph, and R. A. Buhrman, Phys. Rev. Lett. **106**, 036601 (2011).

[42] J.-C. Rojas-Sánchez, N. Reyren, P. Laczkowski, W. Savero, J.-P. Attané, C. Deranlot, M. Jamet, J.-M. George, L. Vila, and H. Jaffrès, Phys. Rev. Lett. **112**, 106602 (2014).

[43] W. F. Zhang, W. Han, X. Jiang, S.-H. Yang, and S. S. P. Parkin, Nat. Phys. **11**, 496 (2015).

[44] V. T. Pham, L. Vila, G. Zahnd, A. Marty, W. Savero-Torres, M. Jamet, and J. P. Attane, Nano Lett. **16**, 6755 (2016).

[45] B. F. Miao, S. Y. Huang, D. Qu, and C. L. Chien, AIP Adv. **6**, 015018 (2016).

[46] C. H. Du, H. L. Wang, F. Y. Yang, and P. C. Hammel, Phys. Rev. Appl. **1**, 044004 (2014).

[47] L. Liu, C.-F. Pai, Y. Li, H. W. Tseng, D. C. Ralph, and R. A. Buhrman, Science **336**, 555 (2012).

[48] K. Chen and S. F. Zhang, Phys. Rev. Lett. **114**, 126602 (2015).

[49] K. Chen and S. F. Zhang, IEEE Magn. Lett. **6**, 3000304 (2015).

[50] P. Deorani and H. Yang, Appl. Phys. Lett **103**, 232408 (2013).

[51] L. Shen, Phys. Rev. Lett. **24**, 1104 (1970).

[52] S. Kevan, Phys. Rev. Lett. **50**, 526 (1983).

[53] S. LaShell, B. A. McDougall, and E. Jensen, Phys. Rev. Lett. **77**, 3419 (1996).

[54] J. Nitta, T. Akazaki, H. Takayanagi, and T. Enoki, Phys. Rev. Lett. **78**, 1335 (1997).

[55] A. Bettac, L. Köller, V. Rank, and K. Meiwes-Broer, Surf. Sci. **402**, 475 (1998).

[56] T. Nussbaumer, Ph. Lerch, E. Kirk, A. Zehnder, R. Füchslin, P. F. Meier, and H. R. Ott, Phys. Rev. B **61**, 9719 (2000).

[57] V. Sokolenko, Y. D. Starodubov, V. Mirny, A. Zavgorodniĭ, B. Merisov, and V. Kozinets, Low Temp. Phys. **29**, 587 (2003).

[58] Y. M. Koroteev, G. Bihlmayer, J. E. Gayone, E. V. Chulkov, S. Blugel, P. M. Echenique, and P. Hofmann, Phys. Rev. Lett. **93**, 046403 (2004).

[59] M. Salvadori, A. Vaz, R. Farias, and M. Cattani, Surf. Rev. Lett. **11**, 223 (2004).

[60] C. R. Ast, J. Henk, A. Ernst, L. Moreschini, M. C. Falub, D. Pacilé, P. Bruno, K. Kern, and M. Grioni, Phys. Rev. Lett. **98**, 186807 (2007).

[61] I. Gierz, T. Suzuki, E. Frantzeskakis, S. Pons, S. Ostanin, A. Ernst, J. Henk, M. Grioni, K. Kern, and C. R. Ast, Phys. Rev. Lett. **103**, 046803 (2009).

[62] K. Yaji, Y. Ohtsubo, S. Hatta, H. Okuyama, K. Miyamoto, T. Okuda, A. Kimura, H. Namatame, M. Taniguchi, and T. Aruga, Nat. Commun. **1**, 17 (2010).

[63] A. Bendounan, K. Aït-Mansour, J. Braun, J. Minár, S. Bornemann, R. Fasel, O. Gröning, F. Sirotti, and H. Ebert, Phys. Rev. B **83**, 195427 (2011).

[64] H. Chang, P. Li, W. Zhang, T. Liu, A. Hoffmann, L. Deng, and M. Wu, IEEE Magn. Lett. **5**, 6700104 (2014).

[65] S. Dutta, K. Sankaran, K. Moors, G. Pourtois, S. Van Elshocht, J. Bömmels, W. Vandervorst, Z. Tőkei, and C. Adelmann, J. Appl. Phys. **122**, 025107 (2017).

[66] R. Ramaswamy, Y. Wang, M. Elyasi, M. Motapothula, T. Venkatesan, X. Qiu, and H. Yang, Phys. Rev. Appl. **8**, 024034 (2017).

[67] X. Tao, Q. Liu, B. Miao, R. Yu, Z. Feng, L. Sun, B. You, J. Du, K. Chen, S. Zhang, L. Zhang, Z. Yuan, D. Wu, and H. Ding, Sci. Adv. **4**, eaat1670 (2018).

[68] J. Varignon, L. Vila, A. Barthélémy, and M. Bibes, Nat. Phys. **14**, 322 (2018).

[69] N. Bobrov, Low Temp. Phys. **45**, 482 (2019).